PREDICTION OF THE AERODYNAMIC CHARACTERISTICS OF FLIGHT VEHICLES IN LARGE UNSTEADY MANEUVERS

Michael R. Mendenhall*
Stanley C. Perkins, Jr.**
Daniel J. Lesieutre+
Nielsen Engineering & Research, Inc.
Mountain View, CA 94043-2287

Abstract

A rational flow model to predict the nonlinear aerodynamic forces and moments on a flight vehicle undergoing steady and unsteady maneuvers at subsonic speeds is described. The major physical flow phenomena over the missile are simulated, including the lee-side separation vorticity. The mutual interaction between the vehicle and the time-dependent flow field is considered in the prediction of the unsteady aerodynamic characteristics at any specified instant in time. The aerodynamic prediction method is coupled with a six-degree-of-freedom equation-of-motion solver to predict missile trajectories, or it is used for models undergoing forced trajectories or oscillating motions. The prediction method is verified by comparison with experimental data where possible.

Nomenclature

c_n	normal-force coefficient per unit length, N/qD
C_p	pressure coefficient
C_m	pitching-moment coefficient
C_N	normal-force coefficient
d,D	diameter
f	pitching frequency
$\vec{i},\vec{j},\vec{k}$	unit vectors in x,y,z-system
I	moment of inertia
K	reduced frequency, $\pi fD/V_\infty$
ℓ	missile length
m	mass
M'	pitching moment
p	rolling rate, and local static pressure
q	pitching rate
q_∞	free stream dynamic pressure, $\frac{1}{2}\rho V_\infty^2$
q'	nondimensional pitching rate, $q\ell/V_\infty$
r	yawing rate
r_o	missile radius
R	radial distance
Re	Reynolds number
t	time
V_∞	free stream velocity
u,v,w	perturbation velocities
W	weight
W(σ)	complex velocity potential
x,y,z	missile coordinate system, origin at CG
x_i,y_i,z_i	inertial coordinate system
X,Y,Z	missile coordinate system, origin at nose
Z'	normal force
α	angle of attack
α'	local angle of attack
α_c	angle between free stream velocity vector and body axis
β	angle of yaw
β'	local angle of yaw
Γ	vortex strength
Δt	time increment
ΔX	axial length increment
θ	polar angle, Fig. 2
ρ	free stream density
φ	roll angle and velocity potential
Φ	velocity potential
ψ	stream function
ω	rotation rate

Subscripts

$(\bar{\ })$	conjugate of complex quantity
$(\ )_{AM}$	apparent mass
$(\ )_B$	body
$(\ )_P$	point P on body
$(\ )_s$	steady
$(\ )_u$	unsteady

Introduction

Operational requirements of modern flight vehicles, both aircraft and missiles, can involve dynamic maneuvers which result in very high angles of incidence and large angular rates. Under such flow conditions, the vehicle experiences important nonlinear aerodynamic forces and moments due to flow separation and roll up of the lee-side vortices (Fig. 1) and induced effects of trailing vorticity from lifting surfaces. In unsteady flow, the strength and position of these vortices and their induced effects are dependent on the history of the motion of the vehicle, and conversely, the motion of the vehicle is dependent on the vortex-induced aerodynamic effects. Prediction of the vehicle motion when the aerodynamic characteristics are dominated by high-angle nonlinear effects requires a different approach from traditional linear prediction methods which are applicable to low-angle unseparated flow conditions. Unsteady nonlinear techniques are required for predicting and understanding the complex flow phenomena involved in high-angle maneuvers.

A rational flow model to simulate the major physical features of the flow around a body of revolution undergoing steady or unsteady motions in incompressible flow is described in this paper. The prediction method is directed at the calculation of nonlinear aerodynamic forces and moments without resort to empirical information; therefore, the method is applicable to general configurations for which experimental data are not available.

The genesis of the aerodynamic method described herein is the discrete vortex cloud model of the lee-side vorticity shed from bodies at high

---

* Vice President and Principal Engineer
** Senior Research Engineer
\+ Research Engineer

angles of attack.[1,2,3] This nonlinear flow model for prediction of static aerodynamic characteristics was extended to handle configurations undergoing steady flow with constant incidence angles and constant angular rotation rates in Ref. 4. Such a flow condition is achieved when a body is moving along a circular-arc path while inclined at a constant angle to the path. Experimentally, this condition is represented by testing a model on a rotating-arm apparatus.

The steady flow model was further extended to include unsteady motion in Ref. 5. The aerodynamic prediction method is coupled to a six-degree-of-freedom equation-of-motion solver for direct calculation of missile trajectories without the need for the complete set of stability derivatives or large quantities of empirical information. The aerodynamic prediction method can also be used if the motion of the vehicle is prescribed, such as a specified turn or a fixed, time-dependent oscillation.

The purpose of this paper is to describe both the extension of the vortex cloud method to unsteady flows and the vehicle trajectory analysis. The following sections include a discussion of the approach to the problem and a description of the analysis and flow models required to carry out the calculations. Where possible, the prediction method is evaluated through comparison of measured and predicted results for a variety of flow conditions. When data are not available for comparisons, predicted results are presented for typical configurations for a range of flow conditions.

General Approach

The rational flow model is an engineering prediction method for flight vehicles maneuvering at high angles of incidence in a flow regime in which the aerodynamic characteristics are dominated by nonlinear effects. The prediction method represents the complex physical phenomena in the flow field adjacent to the vehicle, including both steady and unsteady hull separation vorticity and lifting surface trailing vorticity. Vehicles can have a wide range of configurations and component arrangements, but for purposes of this discussion, the rational flow model is directed at axisymmetric bodies with fore and/or aft lifting surfaces.

The major nonlinear effect on a missile at high angles of incidence in both steady and unsteady flow conditions is the separation vortex wake on the lee side of the body. The vorticity is formed by boundary-layer fluid leaving the body surface from separation lines on both sides of the missile. At moderate angles of attack, the vorticity rolls up into a symmetrical vortex pair (Fig. 1). These vortices induce nonlinear effects which can dominate the aerodynamic forces and moments and thus can have a major influence on the missile trajectory. A successful approach to modeling the lee-side vorticity under static flow conditions is the representation of the vortex wake by a cloud of discrete vortices. As described by this author[1,2,3] and other investigators[6,7,8] the vortex cloud model is a reasonable means to predict a very complex flow phenomenon. The selected approach to the more complex problem of maneuvering missiles will begin with the basic vortex cloud model and extend it to the more complicated unsteady flows.

The calculation of the aerodynamic characteristics of a missile configuration under steady translation and rotation (Fig. 2) is carried out with a marching procedure in the same manner as the static approach.[2,3] The basic discrete vortex shedding model is unchanged; however, the surface pressure calculation and the vortex tracking procedures reflect the fact that the vehicle is in steady flow which is changing along the body. The strength and position of the vortex wake and its induced effect on the body becomes a function of the motion of the vehicle.

The situation is more complex in unsteady flow conditions. The initial conditions, which must be steady, are computed as described above for user-specified velocities, angles, and rates. The predicted forces and moments on the missile are used to calculate the motion of the missile over a small time interval, assuming the forces and moments and flow conditions are constant in the interval. The trajectory calculation produces new flow conditions and time rates of change of flow variables at the end of the interval. The vortex wake is allowed to move downstream under the influence of the changing local flow conditions during the interval Δt, where it influences the pressure distribution and subsequent separation. New vortices are added to the field, new forces and moments are computed, and the calculation procedure is repeated. The vortex wake represents the historical lag in the flow field which relates to the aft portion of the vehicle what happened at an earlier time on the nose. The early positions of the wave are eventually swept downstream past the base of the body and their effect on the induced loads is lost forever.

Details of the flow models and the calculation procedure are described in the following sections.

Methods of Analysis

Geometry

The rational flow model contained in the prediction method is comprised of basic geometry models representing a body and lifting surfaces. A propulsion system is not included in the current analysis. The flow models required to represent the configuration are described in this section.

Body. The fuselage is defined as a body of revolution without appendages, and the volume effects are represented by a series of point sources and sinks distributed on the axis. A three-dimensional singularity distribution provides a potential flow model for calculating velocities at any point in the flow field outside the body surface and for calculating the surface pressure distribution on the surface. This type of three-dimensional representation is described in Refs. 3 and 9 for missile shapes.

Lifting Surfaces. The prediction method described herein permits two regions of lifting surfaces, each region containing multiple lifting

surfaces or fins. A fin may be attached to the body or to another fin as for an end-plate. Each surface is modeled using the vortex-lattice lifting surface method described in Refs. 9 and 10. Horseshoe vortices are distributed on the lifting surface and are imaged inside the constant-radius hull section (Ref. 11). The strengths of the horseshoe vortices are obtained by satisfying the flow tangency condition at control points distributed over the lifting surface. This boundary condition includes induced effects from shed vorticity in the field, the presence of the hull, the impressed flow conditions (including angular rotation), and the image vortex system inside the hull. In addition, the boundary condition includes mutual interference from all lifting surfaces in the region under consideration.

Flow Phenomena

The nonlinear, aerodynamic forces and moments acting on a flight vehicle undergoing maneuvers are associated with many different types of flow phenomena. These phenomena are both the result of and responsible for the nonlinear behavior of the vehicle. The individual components of the flow phenomena of importance are the body nose and afterbody vorticity and the lifting surface trailing vorticity.

First, consider the flow field of the body alone in steady flow. At very low angles of attack, the flow is almost entirely attached to the body with the possible exception of a small separated region near the tail of a body with a boattail. This particular separation region does not form a large wake; thus it does not have a large effect on the induced flow field near the lifting surfaces. As the angle of attack increases, the axial-type separation region at the tail becomes a crossflow-type separation and moves forward on the body. At angles of attack between 10 and 15 degrees, a strong symmetric vortex field occurs on the lee-side of the body as illustrated in Figure 1. This vortex field causes interference on the foremounted and aftmounted lifting surfaces and the body.

When the motion is unsteady, the vortex shedding described above is unsteady, and the vortex wake changes with time. It is necessary to maintain the history of the vortex wake by tracking the location of the vorticity as a function of time.

A major feature of the rational flow model is the discrete vortex wake on the lee-side of the body which is developed in the following manner. The three-dimensional steady flow problem is reduced to a two-dimensional, unsteady, separated flow problem for solution. The two-dimensional solution is carried out in the crossflow plane where the flow about a body in the presence of discrete vortices is obtained. At succeeding intervals of length on the body, the body cross section is changing, and a new vortex pair is shed into the flow field from the separation points. The discrete vortices forming the wake are allowed to move in the flow field under the influences of the free stream flow, the body, and other vortices.

The calculation procedure starts at a crossflow plane near the nose where the potential pressure distribution is computed using the full Bernoulli equation. The boundary layer in the crossflow plane is examined for separation using the modified version of Stratford's laminar or turbulent separation criteria. At the predicted separation points, the strength of the separation vortex is determined by the vorticity flux contained in the boundary layer. The vorticity flux is summed into a single point vortex whose strength is a function of the vorticity, the axial integration interval, and the free-stream flow conditions. The shed vortices are placed in the outer field at such a position that the vortex and its image inside the body exactly cancel the crossflow plane surface velocity at the separation point.

Lifting surfaces on the vehicle contribute to the flow phenomena in the vicinity of the vehicle via the trailing vortex wake associated with their loading. This wake is made up of trailing vorticity representing the span load distribution, a trailing vortex associated with side-edge separation at the tip, a trailing vortex due to a leading-edge separation, and shed vorticity associated with the change in loading with time. These vortices must be included with the body vortex field to properly model the complete wake. Interaction between the body vortices and the vortices from the forward fins will change the entire wake configuration, and this will, in turn, have an effect on the wake-induced interference on the afterbody and modify its loading and subsequent shed vorticity.

The vortex field from the nose, foremounted fins, and afterbody moves aft with the flow to approach the tail fins. The relative position of the vortex field and these fins depends on the motion of the configuration during the time required for the vortices to reach these lifting surfaces. The unsteady loading on the tail fins produces an associated trailing vortex wake similar to that described for the forward fins, including the shed vorticity due to the changing loading. This additional vorticity is included with the existing vortex field and tracked downstream beyond the end of the vehicle.

Aerodynamic Characteristics

The singularity models described in the previous sections provide a means to calculate induced velocities due to the flow field components at field points on and near the vehicle. These velocities, in conjunction with contributions from the free-stream and the angular rotations of the body, are used to calculate pressure distributions on the hull surface and loads on the lifting surfaces. Determination of the component and overall loads on the configuration is discussed in this section.

Pressure Distribution. The pressure coefficient at a point on a body undergoing unsteady motion is

$$C_{p_u} = C_{p_s} - \frac{2}{V_\infty^2} \frac{\partial \Phi}{\partial t} \qquad (1)$$

where C_{p_s} is the instantaneous steady pressure coefficient. This result is obtained by a transformation of the Bernoulli equation from an inertial system to the body-fixed coordinate system (Fig. 3), where the last term in Eq. (1) is the unsteady term in the inertial system caused by the motion of the vehicle and the associated changes in the flow field.

The instantaneous steady pressure coefficient is

$$C_{p_s} = \frac{V^2 - q_r^2}{V_\infty^2} - \frac{2 \cos \alpha_c}{V_\infty} \frac{d\phi}{dX} \tag{2}$$

where V is the speed in the inertial coordinate system of a point P fixed in the moving body system and q_r is the fluid velocity of the same point relative to the body-fixed system.

The components of the fluid velocity at P in the x,y,z system are:

due to body motion,

$$\vec{V}_\infty = - V_\infty \cos\alpha_c \vec{i} - V_\infty \sin\beta \vec{j} - V_\infty \sin\alpha \vec{k} \tag{3}$$

due to body rotation,

$$\vec{\omega} \times \vec{R}_p = (ry - qz)\vec{i} - (pz - rx)\vec{j} + (qx - py)\vec{k} \tag{4}$$

and due to perturbation velocities,

$$\vec{V}' = u\vec{i} + v\vec{j} + w\vec{k} \tag{5}$$

The angles of attack and yaw are

$$\sin\alpha = \sin\alpha_c \cos\phi$$

$$\sin\beta = \sin\alpha_c \sin\phi \tag{6}$$

where α_c and ϕ are vehicle incidence and roll angles, respectively.

The perturbation velocities in Eq. (5) consist of induced velocity components due to body volume effects, shed vortices, and fins on the body if present. From Eqs. (3), (4), and (5) the fluid velocity at P is

$$\vec{q}_r = \vec{V}' + \vec{V}_\infty + (\vec{\omega} \times \vec{R}_p) \tag{7}$$

and the velocity of P with respect to the inertial reference frame is

$$\vec{V} = \vec{V}_{\infty_B} + (\vec{\omega}_B \times \vec{R}_p) \tag{8}$$

The last term in Eq. (2) represents the pressure due to a change in two-dimensional velocity potential from one crossflow plane to the next. This term, in which ϕ is the two-dimensional velocity potential in crossflow planes, is required because of the use of two-dimensional singularities in the crossflow planes associated with the vortex wake shedding model. This term is 'unsteady' in the axial coordinate X, but steady in time. This concept is discussed in greater detail in Ref. 1.

Reformulating Eq. (1) using the components defined in Eqs. (7) and (8), the unsteady pressure coefficient on a body in unsteady motion is

$$\begin{aligned} C_{p_u} = &- \left(\left(\frac{u}{V_\infty}\right)^2 - \frac{2u}{V_\infty} \cos\alpha_c - \frac{2u}{V_\infty}\left(\frac{qz}{V_\infty} - \frac{ry}{V_\infty}\right) \right. \\ &+ \left(\frac{v}{V_\infty}\right)^2 - \frac{2v}{V_\infty} \sin\beta - \frac{2v}{V_\infty}\left(\frac{rx}{V_\infty} - \frac{pz}{V_\infty}\right) \\ &\left. + \left(\frac{w}{V_\infty}\right)^2 - \frac{2w}{V_\infty} \sin\alpha - \frac{2w}{V_\infty}\left(\frac{py}{V_\infty} - \frac{qx}{V_\infty}\right) \right) \\ &- \left(\frac{2 \cos \alpha_c}{V_\infty}\right) \frac{d\phi}{dX} - \frac{2}{V_\infty^2} \frac{\partial \Phi}{\partial t} \end{aligned} \tag{9}$$

where Φ is the full three-dimensional velocity potential.

The singularities making up the rational flow model consist of both two-dimensional and three-dimensional distributions. Each singularity is changing with time and contributes to the unsteady pressure term so long as the velocity potential satisfies the condition at infinity that it is equal to zero or to a constant in the inertial reference frame.

The unsteady terms due to the three-dimensional source/sink distribution and due to the two-dimensional doublet term are obtained analytically. Because of the discrete vortex formulation of the wake and the numerical integration procedure used in wake trajectory calculation, a simple differencing technique is applied to evaluate the unsteady terms representing the vortex wake.

Velocity Field. Velocity components are required for prediction of the missile surface pressure distribution and for vortex trajectory calculations. The development of the individual velocity components is presented in the body-fixed X,Y,Z-coordinate system (Fig. 2). The rational flow model is a hybrid of both two- and three-dimensional flow models; the two-dimensional models are presented first.

Referring to Fig. 2, each crossflow plane on the missile has associated with it a complex potential.

$$W(\sigma) = \phi + i\psi \tag{10}$$

where the complex coordinate is

$$\sigma = Y + iZ \tag{11}$$

Components of the complex potential are as follows.

Crossflow due to uniform α and β:

$$W_1(\sigma) = -i\sigma V_\infty \sin\alpha \tag{12}$$

$$W_2(\sigma) = -\sigma V_\infty \sin\beta \tag{13}$$

where $\sin\alpha$ and $\sin\beta$ are defined in Eq. (6).

The doublet terms representing a cylinder in α' and β' flow are:

$$W_3(\sigma) = i \frac{r_o^2}{\sigma} V'_\infty \sin\alpha' \tag{14}$$

$$W_4(\sigma) = - \frac{r_o^2}{\sigma} V'_\infty \sin\beta' \tag{15}$$

where the equivalent local angles of incidence are

$$\sin\alpha' = \frac{V_\infty \sin\alpha + w_q}{V'_\infty} \tag{16}$$

$$\sin\beta' = \frac{V_\infty \sin\beta + v_r}{V'_\infty} \tag{17}$$

The total free-stream velocity as defined in the crossflow plane is

$$(V'_\infty)^2 = (V_\infty \cos\alpha_c)^2 + (V_\infty \sin\beta + v_r)^2 + (V_\infty \sin\alpha + w_q)^2 \tag{18}$$

where

$$w_q = - (X_{CG} - X)q \tag{19}$$

$$v_r = (X_{CG} - X)r \tag{20}$$

The velocity potentials due to the discrete vortices and their images are

$$W_5(\sigma) = - i \sum_{n=1}^{N} \frac{\Gamma_n}{2\pi} \ln(\sigma - \sigma_n) \tag{21}$$

$$W_6(\sigma) = i \sum_{n=1}^{N} \frac{\Gamma_n}{2\pi} \ln\left(\sigma - \frac{r_o^2}{\bar{\sigma}_n}\right) \tag{22}$$

The total two-dimensional complex potential is given by the sum of Eqs. (12), (13), (14), (15), (21) and (22). The associated velocity components are obtained from

$$\frac{dW(\sigma)}{d\sigma} = v - iw \tag{23}$$

Details of the character of these velocity components are presented in Refs. 1 and 3.

The "unsteady" two-dimensional term in the pressure Eq. (11), is evaluated on the missile surface as

$$\frac{d\phi}{dX} = \text{Real} \left.\frac{dW(\sigma)}{dX}\right|_{r=r_o} \tag{24}$$

where the required complex potential is

$$W(\sigma) = \phi + i\psi = \frac{r_o^2}{\sigma} V'_\infty(-\sin\beta' + i \sin\alpha') + \sum_{n+1}^{N} \frac{\Gamma_n}{2\pi} \left[-i \ln(\sigma - \sigma_n) + i \ln\left(\sigma - \frac{r_o^2}{\bar{\sigma}_n}\right)\right] \tag{25}$$

The other velocity components included are the induced effects of the three-dimensional source and sink distribution[3] and those associated with the steady rotation of the body.

Separation Line. The separation lines on the hull are required to specify the strength and position of the discrete wake vortices forming the feeding sheets. A turbulent boundary-layer separation criteria proposed by Stratford (Ref. 14) has been modified for three-dimensional effects in Ref. 1. The modified turbulent criteria locates separation at the point where the relationship

$$C_p \left(\xi \frac{dC_p}{d\xi}\right)^{.5} (10^{-6} Re_\xi)^{-0.1} = 0.35 \sin\alpha_c \tag{26}$$

is satisfied. Note that C_p is the pressure coefficient referenced to ambient conditions at the minimum pressure point, and ξ is the boundary layer run length measured from a virtual origin.

A laminar separation criterion proposed by Stratford (Ref. 15) and modified for three-dimensional effects[1] locates separation at the point where

$$C_p^{1/2} \left(\xi \frac{dC_p}{d\xi}\right) = 0.087 \sin\alpha_c \tag{27}$$

is satisfied. The constants on the right-hand sides of Eqs. (26) and (27) are nominal values selected from a range of values recommended in Refs. 14 and 15.

Forces and Moments. At a given instant in time, the total forces and moments on a vehicle are given by the sum of the forces and moments on the body and the lifting surfaces.

The instantaneous forces and moments on the body are computed by integration of the pressure distribution around and along the body. At a specified station, the normal-force coefficient on an increment of length of the body is

$$c_n = \frac{1}{D} \int_o^{2\pi} C_{p_u} r_o \cos\theta d\theta = \frac{\text{normal force per unit length}}{q_\infty D} \tag{28}$$

and the total normal-force coefficient is

$$C_N = \frac{D}{S_r} \int_o^{\ell} c_n dX = \frac{\text{normal force}}{q_\infty S_r} \tag{29}$$

The pitching-moment coefficient, positive when the nose is moved vertically upward, is

$$C_m = \frac{D}{S_r} \int_o^{\ell} c_n \left(\frac{X_m - X}{\ell_r}\right) dX \tag{30}$$

The remaining force and moment coefficients in the X, Y, Z-coordinate system are:

side-force coefficient,

$$C_y = - \frac{1}{S_r} \int_o^{\ell} \left(\int_o^{2\pi} C_{p_u} r_o \sin\theta d\theta \right) dX \tag{31}$$

yawing-moment coefficient,

$$C_n = -\frac{1}{S_r}\int_o^{\ell}\left(\int_o^{2\pi} C_{p_u} r_o \sin\theta d\theta\right)\left(\frac{X_m - X}{\ell_r}\right) dX \quad (32)$$

axial-force coefficient, excluding skin friction,

$$C_A = \frac{1}{S_r}\int_o^{\ell}\left(\int_o^{2\pi} C_{p_u} r_o \frac{dr_o}{dX} d\theta\right) dX \quad (33)$$

The circular cross section body does not contribute to the rolling moment.

As described in a previous section, horseshoe vortices are distributed on all lifting surfaces and imaged inside the hull. The loading acting on each lifting surface is calculated using the Kutta-Joukowski law for a force acting on a vortex filament. As described in Ref. 16, the force per unit length, $\vec{F}$, acting on vortex vector, $\vec{\Gamma}$, is given by the vector product

$$\vec{F} = \vec{Q} \times \rho\vec{\Gamma} \quad (34)$$

where $\vec{Q}$ is the total flow velocity vector and ρ is the mass density of the fluid. The total velocity acting on a bound or trailing leg of a horseshoe vortex is made up of induced velocities due to the free stream, the body, the vorticity in the field, and all of the other horseshoe vortices and their images.

Use of Eq. (34) results in forces both normal to and in the plane of each lifting surface. The normal force on a given lifting surface represents the potential force for that surface. The inplane force coefficients are used in conjunction with a method to determine the additional nonlinear lift associated with flow separation along swept leading and side edges. This method, which is an extension of the Polhamus leading-edge suction analogy (Ref. 17), was developed from experimental data and is used to determine the fraction of leading-edge or side-edge suction converted to normal force. This correlation method is described in detail in Ref. 12.

The vortex lattice lifting surface method described above is an attached flow model. Under certain flow conditions, individual surfaces can become very highly loaded due to large onset flows or large vortex-induced velocities, and the predicted loading obtained using the attached flow model may exceed the loading that could physically be expected to occur on the surface. A means to include stall or separation effects on the lifting surface loadings, based in part on the method of Ref. 18, is included in the prediction method.

Maneuver Analysis. A common approach to the prediction of vehicle trajectories involves the integration of the six-degree-of-freedom equations of motion of the configuration over the time frame of interest. The standard equations of motion, such as those presented in Ref. 19, are written in a form which requires the stability derivatives for the configuration for the range of flow conditions to be considered. Such a formulation creates difficulties when the stability derivatives are unknown, as is the case for a preliminary design configuration prior to testing, or when the flight regime involves nonlinear aspects which make it impossible or difficult to determine the derivatives experimentally.

The approach to the development of a trajectory prediction method based on the rational flow model involves a simplification of the standard stability derivative coefficient formulation using a direct force and moment coefficient formulation. In this approach, terms in the equations of motion associated with stability derivatives are replaced by the forces and moments obtained from the rational flow code at an instant in time. The modified equations of motion are shown below. These equations are for a configuration with its origin at the center of gravity, and the positive senses of forces, moments, velocities, and rotation rates are indicated in Fig. 4. The angles ϕ, θ, and ψ are the Euler angles which relate to orientation of the body-fixed-coordinate system to the inertial system. The C_i coefficients and the subscript AM are added-mass terms. The added-mass forces and moments have been removed from the right-hand side of the equations of motion and the appropriate terms included on the left-hand side to remove numerical instability in the solution as discussed in Ref. 20.

Only the normal force and pitching moment equations are presented below; however, the equations for the other planes are developed in a similar manner.

Normal Force:

$$(m - C_5)\dot{w} - C_6\dot{q} = m(uq - vp) + (Z' - Z'_{AM}) + W\cos\theta\cos\phi \quad (35)$$

Pitching moment:

$$(I_{yy} - C_{10})\dot{q} - I_{xy}\dot{p} - I_{yz}\dot{r} - C_{11}\dot{w} = (I_{zz} - I_{xx})rp + (M' - M'_{AM}) \quad (36)$$

A trajectory calculation is carried out in the following manner. Starting with initial flow conditions, rotation rates, time rates of change of these quantities, and the initial position and orientation of the submersible configuration in the inertial coordinate system, a steady flow solution is obtained to provide a vortex wake and aerodynamic forces and moments with which to begin the unsteady calculation. The unsteady calculation begins with the prediction of the missile motion from t=0 to t=Δt, where the time interval Δt must satisfy the relation

$$\Delta t \leq \frac{\Delta X}{(V_\infty \cos\alpha_c)_{t=0}} \quad (37)$$

This interval was chosen to provide sufficient time for the changing vortex effects to influence the calculation before being swept past the base of the vehicle. For purposes of the trajectory calculation, it is assumed that the flow conditions and aerodynamic forces and moments are constant over the Δt interval. Solution of the 6-DOF equations of motion results in new velocity components and coordinates of the configuration CG, angular rates, and orientation of the configuration at t_1.

The vortex wake is permitted to move in the time interval to its new position. With the new wake position and the new flow conditions at t_1, the forces and moments on the vehicles are computed. This interactive process continues to the end of the specified trajectory calculation. The moving vortex wake forms the historical lag in the flow field which relates to the tail what happened at an earlier time at the nose. As the calculation progresses, the wake shed at an earlier time is swept downstream, and the effect on the vehicle is lost forever.

Calculation Procedure

The general steady and unsteady flow calculation procedure used in the rational flow method for a typical configuration is outlined in this section. The calculation procedures for both steady and unsteady flow conditions are applicable to general configurations with arbitrary arrangements of lifting surfaces on an axisymmetric hull.

Steady Flow

The calculation of the aerodynamic characteristics of a flight vehicle undergoing steady translational and rotational motions is carried out with a marching procedure starting at the nose of the vehicle. The basic method is the crossflow plane discrete vortex shedding analysis described in Ref. 1. The calculation begins with the prediction of the shed vortex field and the loads between the nose and the leading edge of the first set of lifting surfaces, the foremounted fins in most cases. The separation vortex field at this axial station influences the loads on these fins, and the lifting surfaces in turn influence the loading on each other and on the body adjacent to the surfaces. A trailing vortex system originating on the lifting surfaces is released into the flow field at the trailing edge, and these free vortices are included as part of the total shed vortex system for the remainder of the calculation.

The path of the entire vortex system is tracked along the length of the hull from the trailing edge of the forward fins to the leading edge of the aft fins. The vortices influence the pressure distribution on the body, which has an effect on the separation points, the shed vorticity from the afterbody, and the body loads. Separation vortices from the afterbody are added to the vortex field between the forward and aft fins.

The vortex field from the nose, foremounted fins, and afterbody influences the loads on the aftmounted fins. The loading on the individual fins produces a trailing vortex system analogous to that from the forward fins, and these vortices are included as part of the shed vortex system which form the wake of the vehicle.

The total forces and moments on the complete vehicle are the sum of the forces and moments on the individual components. For a steady flow condition, the calculation is complete at this point.

Unsteady Flow

The calculation procedure for the prescribed initial flow conditions for an unsteady flow case is essentially the same as that for the steady flow case. Starting at t = 0 with prescribed initial flow conditions, angular rotation rates, accelerations, position of CG and orientation of the vehicle in the inertial coordinate system, and control surface deflections, the loads and the shed vortex field on the configuration are calculated as described in the previous section. This is the starting condition for the unsteady calculation.

Separation vortex fields corresponding to the initial conditions at t = 0 are shown schematically in Fig. 5(a) where only a body is considered for this discussion. The discrete separation vortex positions are shown as dots at each X-station, and their paths are denoted by dashed lines. The individual vortices are identified as $\Gamma_{m,t}$ where the first subscript represents the X-station at which they are shed and the second subscript represents the appropriate time step.

An unsteady calculation begins with the calculation of the submarine motion from $t = t_o = 0$ to $t_1 = t_o + \Delta t$, where Δt is a specified value that must satisfy Eq. (41). The vehicle trajectory is calculated by making the approximation that the flow conditions and loads at t = 0 are constant over the time interval Δt. The trajectory calculation produces new flow conditions and time rates of change of flow variables for $t_1 = t_o + \Delta t$. The existing vortex wake is allowed to move downstream a distance $\Delta X'$ under the influence of new local flow conditions during the interval Δt. The value of $\Delta X'$ is determined from the average conditions at $\Delta t/2$, such that

$$\Delta X' = \Delta t \, (\bar{V}_\infty \cos \bar{\alpha}_c) \qquad (38)$$

where $\bar{V}_\infty$ and $\bar{\alpha}_c$ are average values between time steps. For the wake trajectory calculation, the average flow conditions at $\Delta t/2$ are considered appropriate for the total interval. A new vortex field resulting from a calculation for which $\Delta X' = \Delta X$ is shown in Fig. 5(b). Comparison of parts (a) and (b) of this figure illustrate how individual vortices are moved. In essence, the entire vortex field existing at t_o has been transported downstream a distance ΔX. Under the influence of the actual flow conditions at t_1 and the modified vortex field, the hull pressure distribution is predicted and a new separation calculation is carried out. The current situation at t_1 is shown in Fig. 5(c) where the new vortices are shown as an addition to the previous field. This process continues to the end of the specified trajectory calculation or to the end of the prescribed maneuver.

Results

The ultimate evaluation of the rational flow model described in this paper must be made by comparisons of measured and predicted aerodynamic characteristics on a variety of flow conditions. Comparisons of both steady and unsteady results

are desirable to verify the methodology; however, other than static characteristics, only a small quantity of steady data exists and almost no unsteady data are available for these comparisons. For these reasons, the following results consider only a body alone with no fins. Predicted results for an unsteady maneuver for a body with fins are described in Ref. 21.

Static Characteristics

The method was applied to a missile configuration consisting of a 3-caliber ogive nose and a 7.7-caliber cylindrical afterbody.[22] For purposes of this discussion, all comparisons shown are for α = 15 degrees; however, the entire angle of attack range was investigated, and these results are considered typical.

Measured and predicted axial distributions of normal force are compared in Fig. 6. The agreement is good over most of the missile length; however, near the base, the predicted results appear to agree better with the high Reynolds number measurements than those for the lower Reynolds number. The predicted results for no separation, which correspond to potential flow, are shown as a dashed curve.

The predicted pressure distribution at X/d=7.5 is compared with experiment in Fig. 7. The presence of the lee-side wake has a significant effect on the pressure distribution, and the rational flow model successfully represents the vortex-induced effects. The potential results are shown as a dashed curve.

The total normal-force coefficient is shown in Fig. 8. At lower angles of attack, the predicted results are in good agreement with the low Reynolds number experimental measurements, but at higher angles, it appears that the theory is in better agreement with the high Reynolds number results.

Steady Turning Maneuver

As discussed previously, a steady turning maneuver involves the missile at constant angles and constant angular rates, and such a maneuver is represented experimentally on a rotating-arm apparatus. Measured pressure distributions on a 4:1 ellipsoid body of revolution in a steady turn are available for comparison.[23] Axial pressure distributions on the windward and leeward meridians are shown in Fig. 9 for $q' = -.0717$ and two angles of attack (α = 10° and 20°). The flow is such that the body is at positive angle of attack and it is pitching nose downward in such a way as to increase the local angle at the base. In Fig. 9(b), the effect of the separation vortex is shown to be significant in its effect on the lee-side pressure.

Since similar data on a typical missile configuration are not available, the ogive-cylinder body considered above was selected for a parametric series of calculations. These results are presented in Ref. 24 and will not be repeated herein.

Unsteady Motion

Unsteady force and moment data are not available for comparison purposes, but unsteady results are presented for an ogive-cylinder missile conside/ed in Ref. 25 where flow visualization of the vortex wake is described.

In Ref. 25, a 3-caliber ogive nose and 7-caliber cylinder afterbody model was tested under forced pitching oscillation about its mid point between α = 0 and 30 degrees according to the schedule

$$\alpha(t) = 15° + 15° \sin(2\pi ft + 3\pi/2) \qquad (39)$$

where $2\pi f = 1$. This results in a reduced frequency, K, of 0.2. Photographs of the vortex wake illustrate the vortex shedding characteristics of the model, and these unique experimental results provide heretofore unavailable detail concerning the complex flow phenomena associated with a pitching missile. The photographs are of a plane normal to the free stream velocity vector.

The prediction method was applied to the ogive-cylinder model, and all results presented below were obtained over 1.5 complete cycles of motion to achieve a periodic result. Because of the low Reynolds number of tests, all vortex shedding is assumed to be laminar. The predicted velocity fields described below are in a plane normal to the missile axis.

Photographs of the wake at the X/ℓ = 0.75 station during one cycle are shown in Fig. 10 where it is assumed that t = 0 occurs at α = 0° on an upstroke. Therefore, the changing wake (time increasing) moves down the left hand column of pictures to α = 30° and then moves up the right hand column of pictures on the downstroke to return to α = 0°. Predicted velocity vectors on the right side of the model are shown at corresponding positions. Since the flow is symmetric, both sides of the model are not presented in the predicted figures. In this figure, an attempt was made to align the vertical position of the model in the predictions with the position in the photographs. The velocity field, including vortex induced effects, illustrates the extent of the wake better than a sketch of the discrete vortices.

Though only qualitative comparisons are possible, it appears that the predicted wake has many characteristics in common with the observed wake. For example, at α = 0° on the upstroke, the wake is concentrated near the side of the model. Note that a portion of this wake was actually shed from the nose on the downstroke of the previous cycle. As the model pitches upward, this station moves downward, and the wake moves to the upper side of the missile. The strength of the wake at this station is also changing during the same period. As the model moves through the downstroke toward α = 0° on the right side of the figure, the wake moves down to the side of the model; however, it appears in both the photographs and the predictions that the wake is more concentrated or tightly rolled up in this portion of the cycle. According to the predicted results, the strength of the vortex wake is stronger between α = 10 and 30 degrees on the downstroke than it is at corres-

ponding positions on the upstroke. The strongest vortices at this axial station occur at $\alpha = 0°$.

An excellent discussion of the propagation of separation on a pitching missile is presented in Ref. 25. Based on flow visualization photographs, the observed propagation of separation is shown as the dashed curve (reproduced from Ref. 25) in Fig. 11 for one complete pitching cycle. The predicted separation locations are shown as the solid curve. Arrows are used to denote the pitching direction. The predicted separation locations are defined as the axial stations at which separation first occurs. The predicted locations are always ahead of the measured locations because it is possible to detect much weaker vortices from the theory than are visible in the photographs. For example, on the downstroke, separation occurs at the nose of the missile for the entire stroke; however, these vortices often remain near the body surface until some distance downstream and they would not appear in the side-view photographs which were used to define the dashed curve.

Though force and moment data are not available for the pitching missile, predicted results are presented to illustrate the effect of vortex shedding on the nonlinear aerodynamic characteristics of the model. The predicted normal-force coefficients on the missile are shown in Fig. 12 for both static and pitching conditions. The linear results with no vortex separation effects included are shown in Fig. 12(a). The static condition is the normal slender body theory result. The dashed curve is the predicted total force on the missile including both aerodynamic and apparent mass forces. The solid curve represents only the aerodynamic force.

The nonlinear effects of vortex shedding are shown in Fig. 12(b) where the static results are similar to those shown in Fig. 8. For the pitching missile, the vortex-induced forces have a dominant effect on the total normal-force coefficient. The first cycle, shown as a dashed curve, begins very smoothly on the upstroke, and because the vortex field has not had an opportunity to build in strength, the results up to $\alpha = 10°$ are nearly identical to those shown on the upstroke. The predicted normal force is slightly larger than the linear result, but on the downstroke where the strong vortex field developed on the upstroke is moving along the missile, the total normal-force coefficient is very different from the linear results. The irregularities in the downstroke results in the first cycle are due to numerical difficulties in the vortex tracking. These difficulties carry over to the initial portion of the second cycle; however, they tend to smooth out and a periodic solution develops.

Predicted pitching-moment coefficients are presented in Fig. 13 for the same flow conditions. The results are similar to those described above for normal force; however, the intensity of the vortex-induced effects are less because they are distributed over the entire missile.

Conclusions

An engineering rational flow model to predict the aerodynamic characteristics and motion of a missile in unsteady maneuvers has been investigated. Comparison of measured and predicted static aerodynamic characteristics of a typical missile configuration verify that the principal features of the flow phenomena are well represented at moderate angles of attack above the linear aerodynamic range. The flow models were extended to include steady turning maneuvers, and a series of calculations on a body of revolution illustrate the capability of the method to predict the detailed aerodynamic and flow field characteristics. Finally, the method was extended to consider unsteady flows in a time-dependent calculation of the aerodynamic characteristics of a missile undergoing pitching motion. Comparison of observed and predicted flow field characteristics illustrate the ability of the prediction method to represent the flow phenomena. Predicted forces and moments indicate large vortex-induced effects on the aerodynamic characteristics.

The unsteady prediction method described in this paper has demonstrated the feasibility of an approach in which the nonlinear forces and moments are predicted for use in a direct calculation of the motion of a missile configuration. The method has application in the calculation of missile trajectories for configurations and flow conditions for which stability derivatives are unknown.

Acknowledgement

The preliminary study reported in this paper was funded under a Nielsen Engineering & Research, Inc., IR&D project. Dr. M. Gad-el-Hak supplied the photographs used in Fig. 10.

References

1. Mendenhall, M. R., Spangler, S. B., and Perkins, S. C., Jr.: Vortex Shedding From Circular and Noncircular Bodies at High Angles of Attack, AIAA Paper 79-0026, Jan. 1979.

2. Mendenhall, M. R. and Perkins, S. C., Jr.: Prediction of Vortex Shedding from Circular and Noncircular Bodies in Supersonic Flow, NASA CR-3754, Jan. 1984.

3. Mendenhall, M. R. and Lesieutre, D. J.: Prediction of Vortex Shedding from Circular and Noncircular Bodies in Subsonic Flow, NEAR TR-354, Nov. 1985 (to be published as a NASA CR).

4. Perkins, S. C., Jr., Mendenhall, M. R., and Young, S. W.: Rational Flow Modeling of Submersible Vehicles. Vol. II - RATFLO Program Manual, Nielsen Engineering & Research, Inc. NEAR TR 265, Jan. 1982.

5. Perkins, S. C., Jr. and Mendenhall, M. R.: Hydrodynamic Analysis of Submersible Vehicles Undergoing Large Unsteady Maneuvers - Vol. II - SUBFLO Program Manual, Nielsen Engineering & Research, Inc. NEAR TR 341, Apr. 1985.

6. Marshall, F. J. and Deffenbaugh, F. D.: Separated Flow Over Bodies of Revolution Using an Unsteady Discrete-Vorticity Cross Wake. Part 1 - Theory and Applications, NASA CR-2414, June 1974.

7. Wardlaw, A. B.: Multivortex Model of Asymmetric Shedding on Slender Bodies at High Angles of Attack, AIAA Paper 75-123, Jan. 1975.

8. Deffenbaugh, F. D. and Koerner, W. G.: Asymmetric Wake Development and Associated Side Force on Missiles at High Angles of Attack, Journal of Spacecraft and Rockets, Vol. 14, No. 3, March 1977, pp. 155-162.

9. Dillenius, M. F. E., Perkins, S. C., Jr., and Mullen, J., Jr.: A General Method for Determining the Forces and Moments on Components of Finned Sections of Underwater Vehicles, NSSC - TM 319-81, Dec. 1981.

10. Mendenhall, M. R., Spangler, S. B., Nielsen, J. N., and Goodwin, F. K.: Calculation of the Longitudinal Aerodynamic Characteristics of Wing-Flap Configurations with Externally Blown Flaps, NASA CR-2705, Sept. 1976.

11. Dillenius, M. F. E., Goodwin, F. K., and Nielsen, J. N.: Extension of the Method for Predicting Six-Degree-of-Freedom Store Separation Trajectories at Speeds up to the Critical Speed to Include a Fuselage with Noncircular Cross Section. Vol. I - Theoretical Methods and Comparisons with Experiment, AFFDL Report TR-74-130, Nov. 1974.

12. Mendenhall, M. R. and Nielsen, J. N.: Effect of Symmetrical Vortex Shedding on the Longitudinal Aerodynamic Characteristics of Wing-Body-Tail Combinations, NASA CR-2473, Jan. 1975.

13. Bollay, W. A.: Nonlinear Wing Theory and its Application to Rectangular Wings of Small Aspect Ratio, ZAMM, Vol. 19, 1939.

14. Stratford, B. S.: The Prediction of Separation of the Turbulent Boundary Layer, Jour. of Fluid Mech., Vol. 5, 1969, pp. 1-16.

15. Cebecci, T., Mosinskis, G. J., and Smith, A. M. O.: Calculation of Viscous Drag and Turbulent Boundary-Layer Separation on Two-Dimensional and Axisymmetric Bodies in Incompressible Flow, McDonnell Douglas Report No. MDC JO 973-01, Nov. 1970.

16. Milne-Thomson, L. M.: Theoretical Hydrodynamics, Fifth Edition, MacMillan Co., 1968.

17. Polhamus, E. C.: Prediction of Vortex-Lift Characteristics Based on a Leading-Edge Suction Analogy, AIAA Paper 69-1133, Oct. 1969. (Journal of Aircraft, Vol 8, No. 4, Apr. 1971, pp. 193-199).

18. McDonnell-Douglas Aircraft Co.: USAF Stability and Control DATCOM, Revised Apr. 1978, Section 4.1.1.4.

19. Etkin, B.: Dynamics of Flight, John Wiley & Sons, Inc. New York, 1959.

20. Lloyd, A. R. J. M.: Progress Towards a Rational Method of Predicting Submarine Maneuvers, RINA International Symposium on Naval Submarines, Vol. II, Paper 21, London, May 1983.

21. Mendenhall, M. R. and Perkins, S. C., Jr.: Prediction of the Unsteady Hydrodynamic Characteristics of Submersible Vehicles, Fourth International Conference on Numerical Ship Hyrdodynamics, National Academy of Sciences, Sept. 1985.

22. Tinling, B. E. and Allen, C. Q.: An Investigation of the Normal-Force and Vortex-Wake Characteristics of an Ogive-Cylinder Body at Subsonic Speeds, NASA TN D-1297, April 1962.

23. Jones, R.: The Distribution of Normal Pressures on a Prolate Spheroid, ARC R&M 1061, Dec. 1925.

24. Mendenhall, M. R., Perkins, S. C., Jr., and Lesieutre, D. J.: Prediction of the Nonlinear Aerodynamic Characteristics of Maneuvering Missiles, AIAA Paper 85-1776-CP, Aug. 1985.

25. Gad-el-Hak, M. and Ho, Chih-Ming: Unsteady Flow Around an Ogive-Cylinder, AIAA Paper 86-0572, Jan 1986.

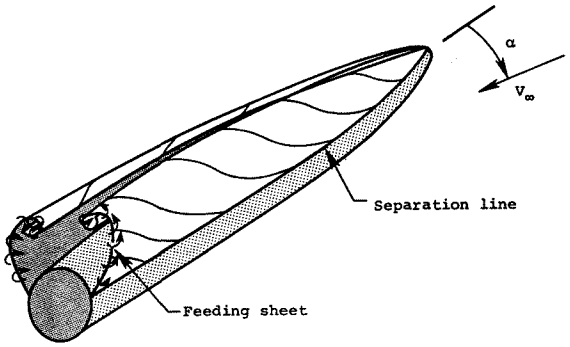

Fig. 1 Vortex formation on an inclined body

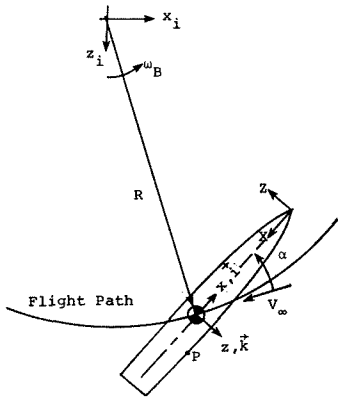

(a) Pitch-plane nomenclature

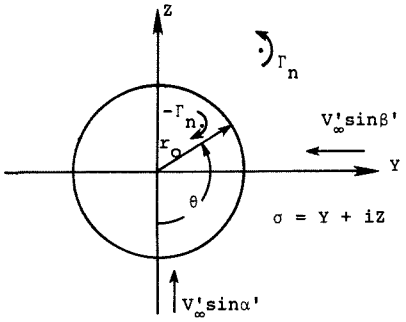

(b) Crossflow-plane nomenclature

Fig. 2 Missile coordinate system for steady flow

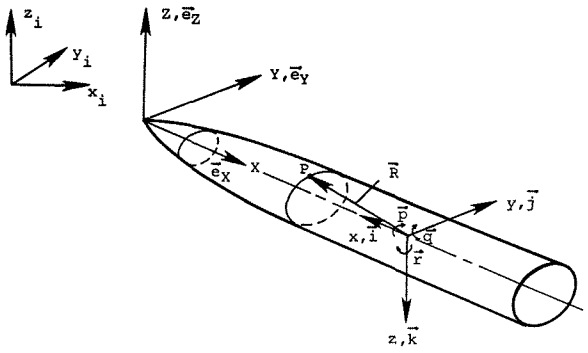

Fig. 3 Coordinate systems and nomenclature associated with pressure coefficient calculation

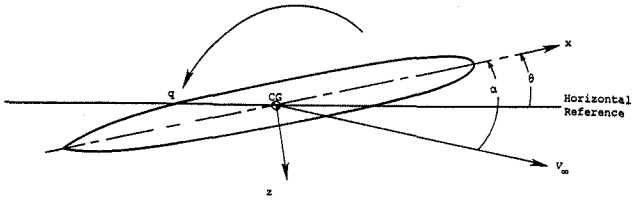

Fig. 4 Sketch showing positive directions of axes, angles, velocities, forces and moments for body-fixed x,y,z coordinate system

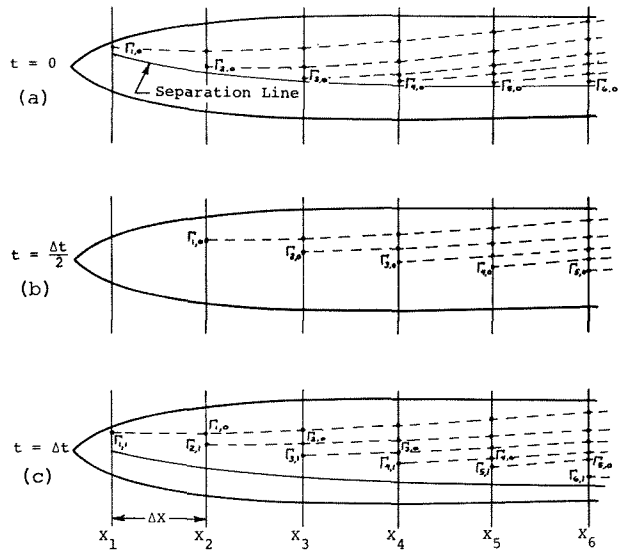

Fig. 5 Unsteady vortex tracking procedure

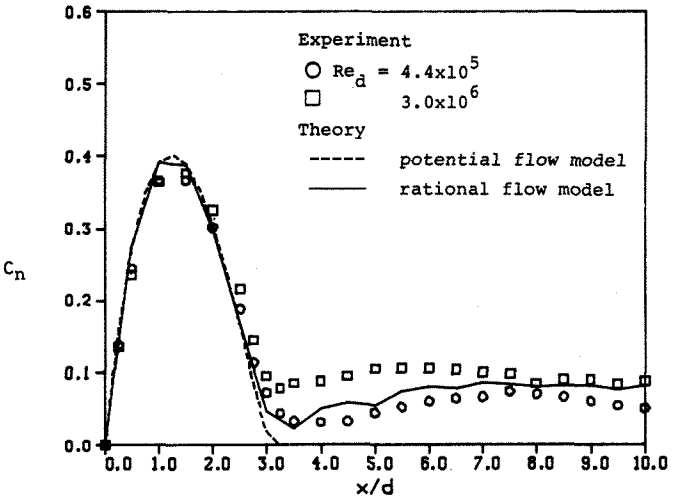

Fig. 6 Measured and predicted normal force distribution on an ogive-cylinder missile, α = 15°

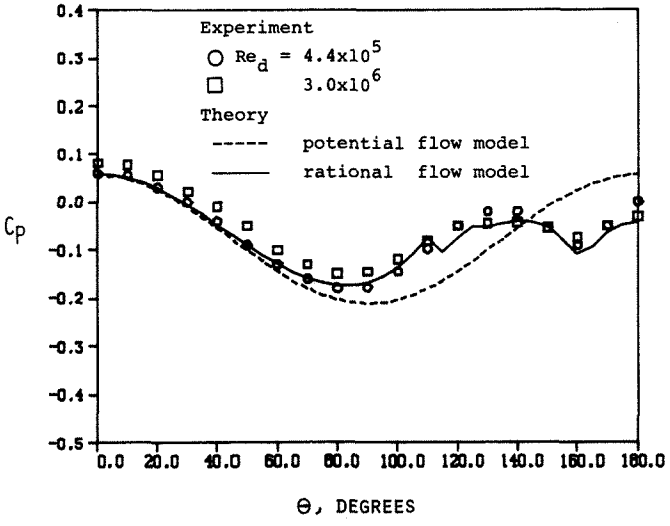

Fig. 7 Measured and predicted pressure distribution on an ogive-cylinder missile, x/d = 7.5, α = 15°

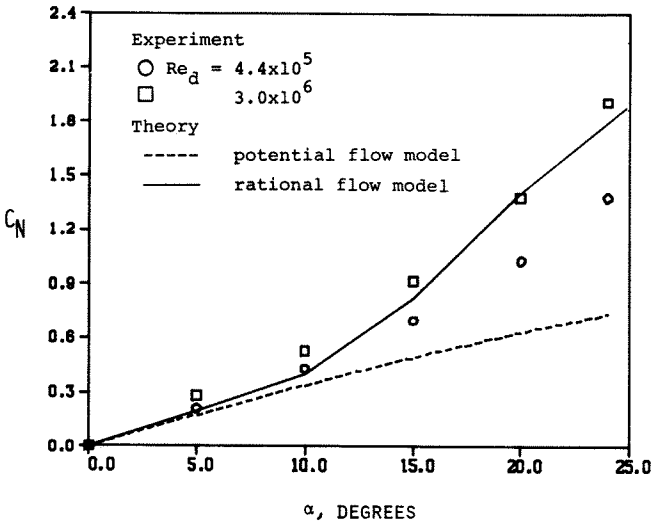

Fig. 8 Measured and predicted normal-force coefficient on an ogive-cylinder missile

Fig. 10 on next page

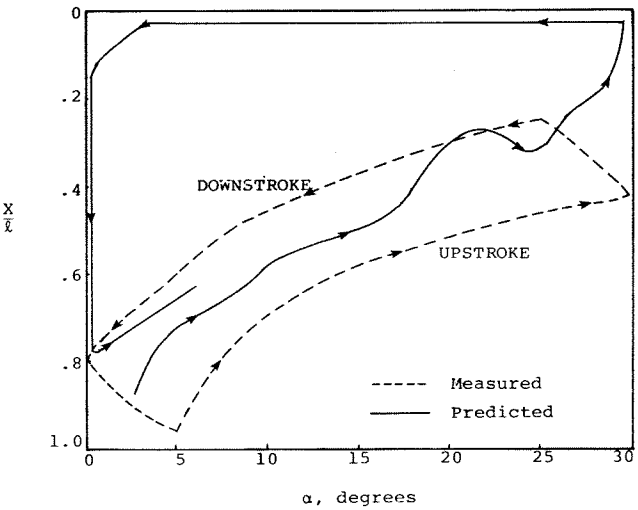

Fig. 11 Measured and predicted propagation of lee-side separation on an ogive-cylinder undergoing pitching motion, K = 0.2

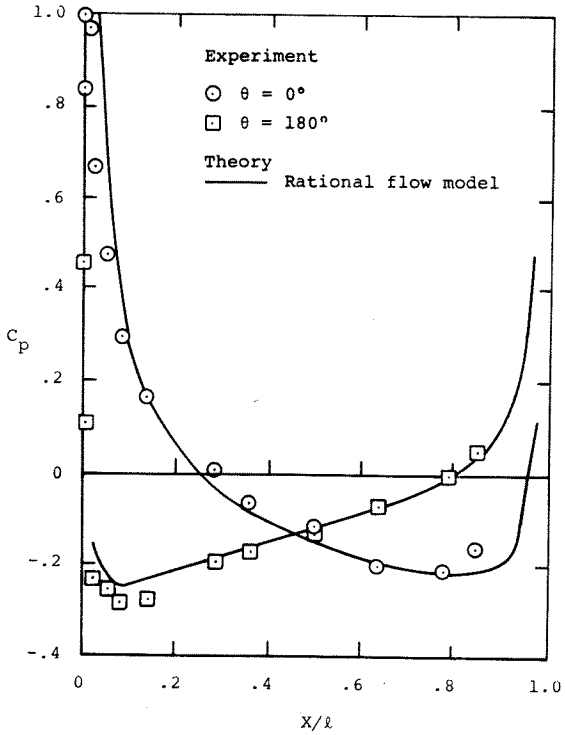

(a) α = 10°, q' = -.0717

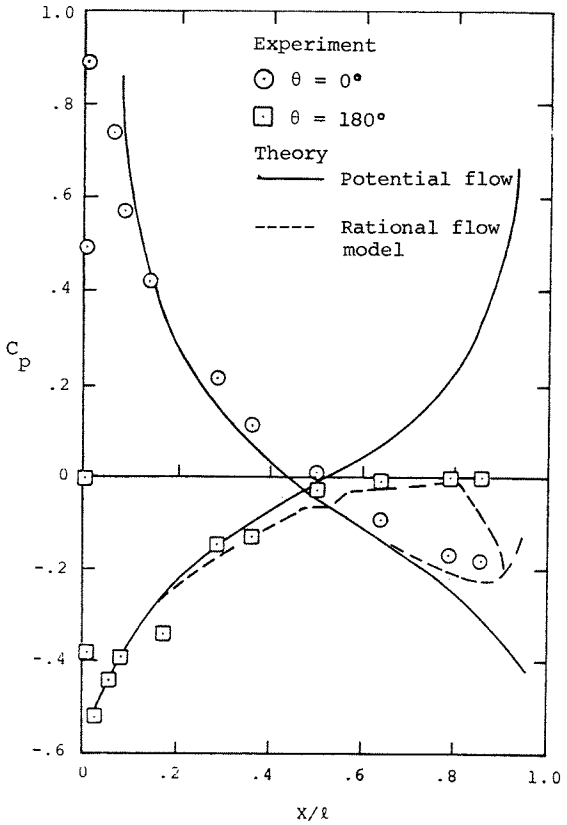

(b) α = 20°, q' = -.0717

Fig. 9 Measured and predicted pressure distribution on a 4:1 ellipsoid body in a steady turning maneuver

Fig. 9 Concluded

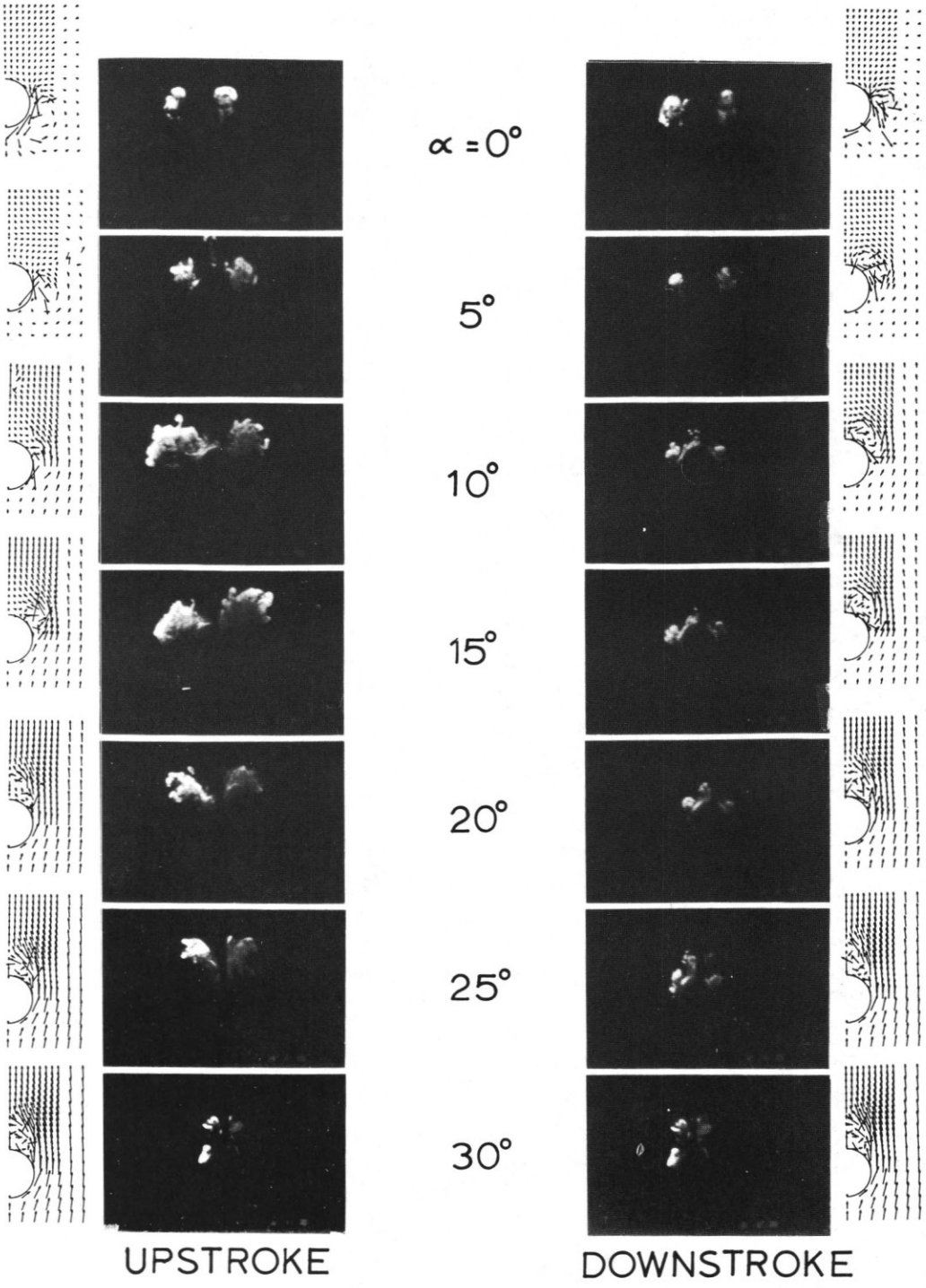

Fig. 10 Vortex wake at X/ℓ = 0.75 on an ogive-cylinder undergoing pitching motion, K = 0.2

Fig. 11 on page preceeding Fig. 10

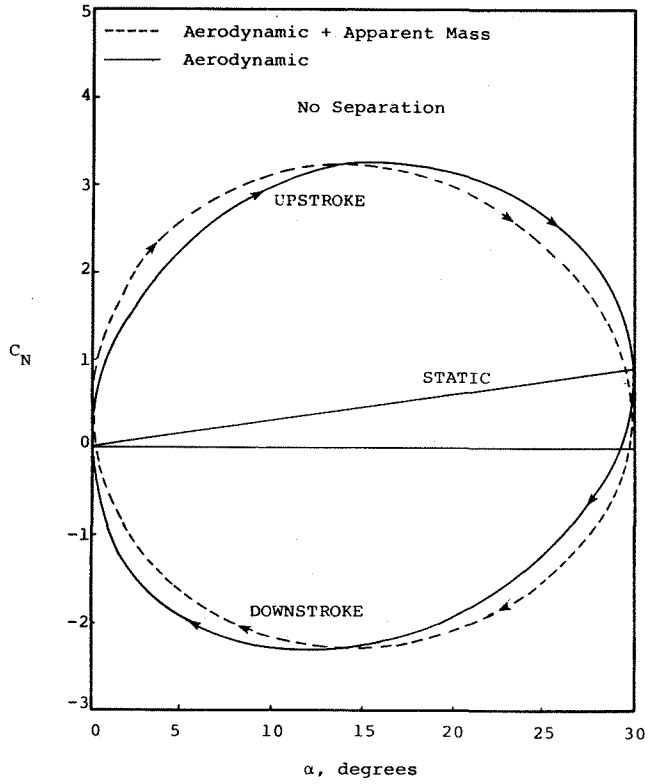

(a) Linear result, no separation

Fig. 12 Predicted normal force on an ogive-cylinder undergoing pitching motion, K = 0.2

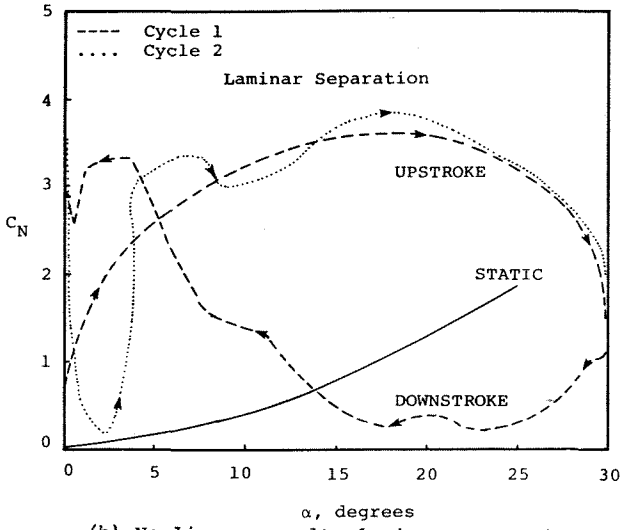

(b) Nonlinear result, laminar separation

Fig. 12 Concluded

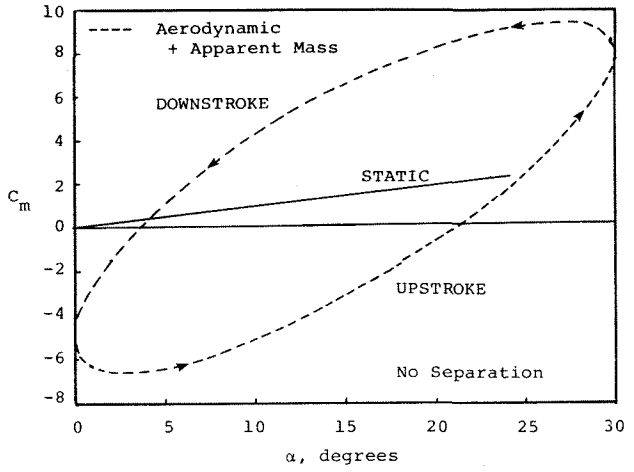

(a) Linear result, no separation

Fig. 13 Predicted pitching moment on an ogive-cylinder undergoing pitching motion, K = 0.2

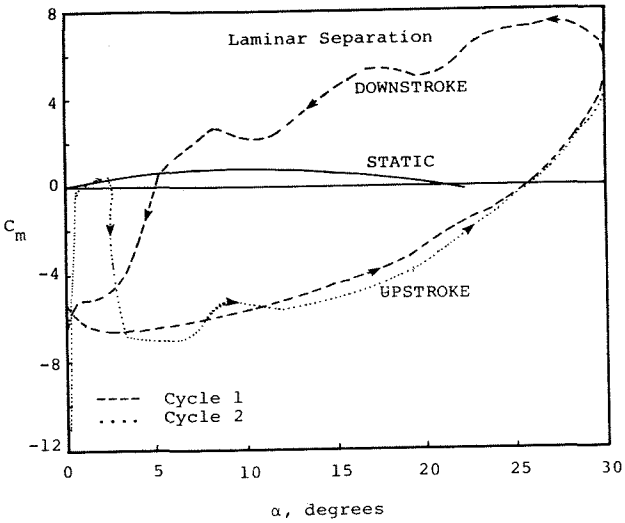

(b) Nonlinear result, laminar separation

Fig. 13 Concluded